Distinct representational roles of distributed cortical regions for working memory storage

Vivien Chopurian[*,1,2], Simon Weber[2,3], Thomas Christophel[*,1,2]

[1]Department of Psychology, Humboldt-Universität zu Berlin, Berlin, Germany

[2]Bernstein Center for Computational Neuroscience Berlin and Berlin Center for Advanced Neuroimaging, Charité Universitätsmedizin Berlin, corporate member of the Freie Universität Berlin, Humboldt-Universität zu Berlin, and Berlin Institute of Health, Berlin, Germany

[3]Research Training Group "Extrospection" and Berlin School of Mind and Brain, Humboldt-Universität zu Berlin, Berlin, Germany

[*]Corresponding authors. E-mail: vivien.chopurian@hu-berlin.de; tbchristophel@gmail.com

Number of figures: 7

Number of tables: 1

Number of multimedia: 0

Number of 3D models: 0

Word counts

Abstract: 179

Introduction: 428

Discussion: 737

Acknowledgements

VC and TC were supported by a DFG Emmy Noether Research Group Grant CH 1674/2-1 to TC. SW was funded by the DFG Research Training Group 2386. We thank Andreea Gui, Damla Cifci, Joana Seabra and Zhiqi Kang for their support with the fMRI data collection and the participants for their participation in this study. We thank Andreea-Maria Gui and Myriam Hamon for their work on the simulation toolbox and Karolis Degutis for sharing his code for the cluster analysis. We thank Alessandra Souza, Christoph Bledowski, Philipp Deutsch and Rosanne Rademaker for their helpful input in discussions about the experimental design and data analysis.

Running title

Distributed visual working memory storage

Competing interests

The authors declare no competing financial interests.

Abstract

While distributed cortical areas represent working memory contents, their necessity for memory maintenance has been questioned. To understand whether these regions serve separable roles when multiple items are maintained, we examined the effect of visual working memory load on neural information across cortical regions. In each trial of the fMRI experiment, participants (N=81) had to memorize two items, each either an orientation or a pure pitch, for 13.8s and continuously recalled the target after the delay. We kept the overall working memory load constant, but varied the sensory modality of each item to vary the effective visual load. We show that increasing visual load decreased behavioural recall performance for orientations and continuous orientation-specific decodable information in visual cortex but not in frontoparietal areas. Simulations show that this selective drop in decodable information is best interpreted as a drop in mnemonic information represented by patterns of visual cortex activity. Our results provide evidence for distinct roles of visual cortices, where single orientations can be stored with high fidelity, and anterior cortices, where multiple orientations could be represented in distinct cortical patterns.

Keywords: fMRI; visual working memory; capacity; MVPA

Significance statement

This study investigated the role of these distributed regions for maintaining multiple items in working memory. We find that orientation information could be decoded in visual and frontoparietal areas for low and high visual load. However, a visual-load-dependent decline in decoding accuracy during the maintenance period was only observed in visual but not frontoparietal areas. Our results highlight the interplay between different cortical regions for the maintenance of multiple working memory items.

Introduction

Working memory capacity is limited. The precision of recall decreases as we increase the number of items to remember (Luck and Vogel, 1997; Gorgoraptis et al., 2011; Ma et al., 2014). In neuroimaging studies, the load dependent decrease in recall performance is accompanied by a decline in the strength of visual working memory representations (Emrich et al., 2013; Sprague et al., 2014; Sutterer et al., 2019). While this evidence demonstrates a link between the ability to decode cortical representations and the capacity to memorize information, it remains unclear whether different cortical regions play distinct roles as memory load increases.

Previous studies highlight a distributed network of sensory, parietal and frontal regions to maintain memorized contents during working memory delay (Fuster, 1998; D'Esposito, 2007; Ester et al., 2015; Christophel et al., 2017; Xu, 2023). For single visual items, studies have found correlations between decodable information in visual cortex and recall performance across participants and trials (Ester et al., 2013; Hallenbeck et al., 2021; Weber et al., 2024). The neuronal selectivity in visual cortex might enable the maintenance of highly detailed, sensory-like, representations of memorized content (Serences et al., 2009; Ester et al., 2013; Harrison and Tong, 2009). These representations have been found to be susceptible to visual distractors, leading to reduced delay-period decoding if the distractors also affected working memory recall (Hallenbeck et al., 2021; Lorenc et al., 2018; Rademaker et al., 2019). Furthermore, imaging and single-cell studies demonstrate the maintenance of item-specific representations in parietal and prefrontal regions (Fuster and Jervey, 1981; Funahashi et al., 1989; Goldman-Rakic, 1995; Ester et al., 2015; Bettencourt and Xu, 2016). In non-human primates, persistent delay activity in the prefrontal cortex directly correlated with behavioural performance (Constantinidis et al., 2001; Wimmer et al., 2014). Presumably, anterior regions maintain abstracted, sensory-modality independent mnemonic representations (Spitzer and Blankenburg, 2012; Leavitt et al., 2018; Yan et al., 2023), which appear to be protected from interference during visual distraction (Ester et al., 2015; Bettencourt and Xu, 2016; Rademaker et al., 2019; Hallenbeck et al., 2021; Lorenc et al., 2018).

However, if multiple low-level visual items have to be encoded and maintained in working memory, their representations are likely to compete for resources in visual cortex (Franconeri et al., 2013). Prior work demonstrates that the extent of cortical overlap of multiple representations predicts the degree to which memory recall is impaired (Cohen et al., 2014). Therefore, we assume that working memory contents from different sensory modalities should interfere less because these representations share little overlap within sensory regions (Baddeley, 2003; Kiyonaga and D'Esposito, 2020). The recruitment of abstract anterior representations (e.g., verbal labels, cat-

egories) could reduce interference by helping to separate similar sensory representations (Wing et al., 2022; Overkott and Souza, 2022; Chunharas et al., 2023) at the cost of precision.

In this study, we investigated the effect of visual working memory load on these distributed cortical representations. We show, by keeping the overall working memory load constant at two items but varying the sensory modality of each item, that increasing visual working memory load selectively reduced continuous mnemonic information about items present in visual cortex but not in anterior regions. Our results provide evidence for a division of labor, where visual cortex is representing individual items and anterior regions support the maintenance of multiple items.

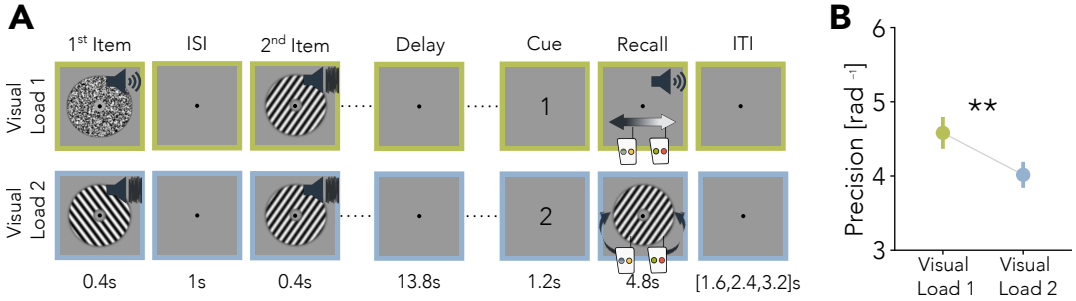

Figure 1: Task setup and behavioural results. **A** Example experimental trials with varying visual load. The top row shows a visual Load 1 trial, where items from both modalities are shown and the target modality is auditory. The bottom row shows a visual Load 2 trial, where both items are visual. Auditory Load 2 trials (not shown) are included in the design to balance the behavioural task. Visual samples were presented jointly with auditory noise and auditory samples were presented with visual masks. **B** Behavioural results for visual targets. Asterisks indicate significance levels of $^{**}p < .01$. Error bars show the SEM.

1 Methods

Participants

Eighty-six participants were scanned. Four data sets with incomplete recordings (resulting from participant dropouts) and one data set with image artifacts (due to a technical failure of the recording setup) were removed from the analysis. Our final sample consisted of 81 participants (48 female, 4 left handed, $mean_{age} = 25$, $sd_{age} = 4$). All participants provided their informed consent and were compensated with 10€ per hour for their participation. The study was approved by the ethics committee of the Humboldt Universität zu Berlin (id: 2022-40) and conducted according to the principles of the Declaration of Helsinki (World Medical Association, 2013).

Task and Procedure

In each trial of the delayed-estimation task, participants had to memorize two sequentially presented items (0.4s, inter-stimulus interval 1s), either two visual orientation stimuli, two auditory pitch stimuli or one of each. Crucially, this means that overall working memory load was constant at two items, but unisensory visual load varied between one or two items (see Figure 1). We focused all our analyses on decoding visual stimuli but included the auditory-auditory condition (auditory Load 2) to balance the design behaviourally. Whenever a sample of a given modality was presented, the other modality was masked. After an extended delay (13.8 s), a visual retro-cue ('1' or '2' for 1.2s) indicated whether the first or second item had to be recalled. During the continuous recall phase (4.8s), participants had to adjust a probe orientation or pitch to match the target item by pressing the inner left and right button, and after confirming their response the fixation dot turned green. The next trial started after a brief period of fixation (1.6, 2.4 or 3.2s).

The experiment consisted of 192 trials, divided in four runs with short breaks in between. The item modality was counterbalanced across cued and non-cued items and 12 orientations and pitches were counterbalanced for each modality and randomized across each cued and non-cued items (see Stimuli). Thus, the two orientations in each load condition were independent from one another (see also Figure 1-1). We randomized the experimental conditions within each scanner run to minimize effects of biased training sets for the cross-validation procedure (see fMRI Analyses). Before the main experiment, participants read instructions presented inside the scanner and completed 12 training trials during an anatomical scan. During these training trials, participants received feedback about their performance as the difference between their response and the target item.

Stimuli

Stimuli were generated with MATLAB and Psychtoolbox-3 (Brainard and Vision, 1997). The background color was set to grey (RGB [128,128,128]). The fixation dot (radius = 0.1°) was centered on the screen. Orientation stimuli and masks were presented as annuli with a total diameter of 7°, an inner diameter of 1.5°. The visual stimuli consisted of 12 orientations with a 15° distance, from 7.5° to 172.5°, and excluded the cardinal axes, with gaussian blur (gaussian kernel = 1°, sd = 0.5°) on all edges. The spatial frequency was set to one cycle per degree. Visual masks were generated by filtering white noise to only include spatial frequencies between 1 and 4 cycles per degree (code from (Rademaker et al., 2019)). During the recall, participants could select their response out of orientations between 1° to 180°, with a precision of 1°. For the auditory stimuli we used 12 pure tones with a distance of one semitone, between 251.63Hz and 493.88Hz, with a

logarithmic ramp up and down of 0.02 seconds. White noise was chosen as auditory masks. The volume was adjusted for participants comfort level. During the recall period, a random pitch was played, and participants could select a response between 246.93Hz and 523.24Hz, with a precision of $\textit{Frequency} \times 2^{\pm 1/(70/1)}$. During the recall phase, a longer button press increased the response step size, making it easier for participants to select their response.

Magnetic resonance imaging

Imaging data was recorded on two 3-Tesla Siemens Prisma MRI scanners with a 64 channel head coil. The first 40 participants were scanned at the Berlin Center for Advanced Neuroscience (Charité Berlin, Germany) with the Syngo MR VE11C operating system, a viewing distance of 148cm and screen of dimensions of 52 x 39cm. The subsequent 41 participants at the Center for Cognitive Neuroscience Berlin (Freie Universität Berlin, Germany) with the Syngo MR XA30 operating system, a viewing distance of 106cm and screen of dimensions of 48 x 27.2cm. Stimulus size was adjusted according to the screen-size and viewing distance, so that all participants received the same visual input. The decoding results for both scanners did not differ qualitatively from the combined results. At the beginning of each session, we recorded T1-weighted MPRAGE structural image (208 sagittal slices, TR = 2400 ms, TE = 2.22ms, flip angle = 8°, voxel size = 0.8mm^2 isotropic, field of view = 240*256 mm). For each of the four runs, we recorded functional images with a multi-band accelerated echo planar imaging sequence, with a multi-band factor of 8 (TR = 800ms, TE = 37ms, flip angle = 52°, voxel size = 2 mm^2 isotropic, 72 slices, 2mm inter-slice gap, field of view = 1872mm).

Preprocessing

All preprocessing steps and analyses were performed in MATLAB, using SPM12 (Ashburner et al., 2014), The Decoding Toolbox (Hebart et al., 2015), and in-house software. First, we converted the acquired DICOM images into NIfTI format. The intensity-normalized anatomical image (T1) was coregistered to the first functional image of the first run for each participant. During segmentation, we estimated the normalization parameters to the Montreal Neurological Institute (MNI) standard space. Functional images were spatially realigned to the first image of the first run and resliced. To remove slow signal drifts accumulating across each run, we applied a cubic spline interpolation to each voxel's time series ($n_{\text{nodes}} = 24$). Afterwards, we applied temporal smoothing by running a moving average of 5 TRs to the data of each run. We used the detrending algorithm and moving average as described in (Weber et al., 2024).

Identifying ROIs

We focused on the distribution of representations across three regions of interests (ROI) using probabilistic maps of retinotopic regions of the human neocortex (Wang et al., 2015). To generate a mask for visual cortex, we combined maps for areas V1 to V3 in standard space. To obtain the bilateral IPS mask, we combined IPS1 to IPS6 from the same probabilistic atlas, and similarly, for the sPCS left and right hemispheres were combined into one mask. After transforming these maps into single-participant space by applying the inverse normalization parameters estimated during preprocessing, we excluded voxels that had less than a 10% probability to belong to each ROI respectively. Secondly, we obtained activity driven maps by estimating a participant-level univariate GLMs for onsets of every orientation presented. After contrasting visual (orientation) activation and baseline, we selected the 1000 most active voxels within the participant-level anatomical ROIs.

fMRI Analyses: pSVR

We analyzed fMRI data using support vector regression (SVR) (Chang and Lin, 2011) to continuously reconstruct memorized orientations. The orientation labels were transformed from the 0°-180° space into radians from -pi to pi. This angular orientation labels (θ) was then projected into sine and cosine labels. This provided a linear measure of these orientations and we predicted each set of these new labels from the multivariate voxel pattern of each ROI with a SVR with a radial basis function kernel (periodic SVR, (Weber et al., 2024)). In each cross-validation fold, we rescaled the training data voxel activation to 0-1 and applied the estimated scaling parameters to the test data. The orientation label was reconstructed by using the four-quadrant inverse tangent:

$$\hat{\theta} = atan2(\widehat{sin(\theta)}, \widehat{cos(\theta)}). \tag{1}$$

We calculated the circular absolute difference between presented and predicted orientation label:

$$\Delta x = |(\theta - \hat{\theta})_{circular}| \tag{2}$$

and this difference was then transformed into a trial-wise feature continuous accuracy (FCA) above chance (Degutis et al., 2024; Pilly and Seitz, 2009; Weber et al., 2024):

$$FCA = 100 - \frac{\Delta x}{pi} \times 100. \tag{3}$$

We subtracted 50% from the resulting FCA, so that 50% refers to chance level decoding with

an error of 45°. All pSVR analyses were run for each TR individually and cross-validated across the four runs. An example of the predicted orientations for each presented orientation are shown for the peak perceptual TR in Figure 2-1C for single orientations in Visual Cortex. On each cross-validation iteration, we trained on the trials of the three runs and tested on the left-out run. In order to increase computational power, we combined all orientations within each of the load conditions (Figure 2A). To investigate effects of serial order, we separated the first and second items after the decoding. For the temporal generalization analysis (Figure 4), we trained the pSVR on each time-point and tested on each time-point, both within and across load conditions.

Statistical analyses

We analysed the behavioural data for the orientation recall by calculating precision ($\frac{1}{sd}$ in radians) for the angular difference between target orientation and response orientation for each condition and participant. We subtracted chance level ($\frac{pi}{4}$), so that an error of 0 corresponds to responses at random (Gorgoraptis et al., 2011). We compared the average of each visual load condition with paired two-sided t-tests.

To test for significant differences in decoding accuracy between the load conditions (visual Load 1 and 2), we used paired two-sided t-tests. In particular, we tested decoding accuracy during a period early in the delay, where we assume to find perceptual activation mixed with memory representations (due to hemodynamic lag), and a period later in the delay, where we assume to find information about mnemonic representations without a substantial influence of perceptual representations. We averaged decoding accuracy per participant in each of these two sections of the delay period (early delay: 7.2s-11.2s; late delay: 12s-16s). Then we tested for the difference between the load conditions within each delay period with paired two-sided t-tests and within each condition for decoding accuracy above chance (50%) with two-sided t-tests. We focused all our other analyses on the late delay. Where applicable, for example when comparing results across ROIs or order and load conditions, we corrected for multiple comparisons with Bonferroni correction. For descriptive purposes, we also compared decoding accuracy to chance level and between conditions (Figure 2B) with two-sided t-tests for each time-point (22 TRs), from the onset of the first stimulus to recall onset. Both analyses were validated with leave one run out cross-validation across participants. Correlation coefficient refers to Pearson's correlation. Correlations were compared with the R package cocor (Diedenhofen and Musch, 2015) and report the p-values for Pearson and Filon's z.

Simulations

We simulated data for a single time point with the same experimental parameters as in our fMRI experiment (N = 81, n runs = 4, n labels = 12, n trials$_{\text{Load 1}}$ = 96, n trials$_{\text{Load 2}}$ = 48, n voxels = 1000) and 1000 iterations for each condition. As in our experiment, we decoded both labels from the Load 2 data, so that both load conditions consisted of 96 trials.

First, we defined the similarity of the orientation space with 12 cosine functions raised to the power of 11 (Sprague et al., 2019), covering the whole orientation space (0°-180°) and their centers set at each stimulus label. Next, we defined a weight matrix (W) for each participant. This weight matrix models the voxel sensitivity for the orientation space and stays constant for each participant throughout the iterations. The noise is white noise sampled from a normal distribution with mean $\mu = 0$ and $\sigma = 1$ (Welvaert and Rosseel, 2014):

$$noise \sim \mathcal{N}(\mu, \sigma^2)\,. \tag{4}$$

We simulated the different load conditions with different *noiseFactors* (5.5, 8, 11.5, 13) to a *signalFactor* of 1, which weights the noise and signal respectively, to approximate our empirical level of decoding accuracy (refers to signal strength of 18.18, 12.5, 8.69 and 7.69% respectively). The simulated multivariate voxel pattern for a single orientation can thus be described as:

$$activity = (W \times basisfunctions) \times signalFactor \tag{5}$$

$$data = activity + noise \times noiseFactor. \tag{6}$$

We simulated the effect of additive data with increased working memory load (Load 2 -Capacity 2), where we generated the multivoxel pattern for each orientation label and then added two patterns (see also Botvinick and Watanabe (2007)):

$$data_{Load2} = (activity_{orientation1} + activity_{orientation2}) + noise \times noiseFactor. \tag{7}$$

Additionally, we simulated a capacity of one by randomly selecting the pattern for one of the items in each trial before adding the two patterns (Load 2 -Capacity 1; see Sutterer et al. (2019)).

In our data, FCA drops from Load 1 to Load 2 by a factor of 2 in V1-V3. To investigate which simulated load 2 condition matches this ratio, we calculated the ratio of Load 1/Load 2 for each of our simulated load conditions and signal strength:

Ratio Load 1/Load 2			
Signal strength [%]	sim. Load 2-Capacity 2	sim. Load 2-Capacity 1	Empirical data
18.18	1.15	4.38	V1-V3: 1.89
12.5	1.13	4.46	IPS: 1.18
8.69	1.11	4.48	sPCS: 1.16
7.69	1.11	4.12	

Table 1: Simulated Load 1/Load 2 ratios compared to empirical data. Signal strength refers to the ratio between Noise factors 5.5, 8, 11.5 an 13 to a Signal factor of 1.

For Figure 3D, we divided our empirical FCA for Load 1 by the ratio based on signal strength for each delay period and ROI in Load 1 (Late delay: V1-V3 = 12.5%, IPS = 8.69%, sPCS = 7.69%).

Temporal generalization analysis

We applied a cluster-based test (Maris and Oostenveld, 2007) for the temporal generalization analyses. First, we generated a null distribution by randomly assigning the sign of the above-chance decoding accuracy matrix for each time-point, over 1000 iterations. Within the permutation test, the summed t-value for the largest cluster within null distribution was calculated and compared to our empirical data with a threshold of $p < 0.05$.

Here, dynamic clusters were defined as elements where an above chance off-diagonal element of the cross-temporal decoding matrix was significantly smaller than its two corresponding diagonal elements ($a_{ij} < a_{ii}$ and $a_{ij} < a_{jj}$). Each of these conditions was tested with a cluster-based permutation test, where we subtracted the diagonal element from the off-diagonal element ($a_{ij} - a_{ii}$ and $a_{ij} - a_{jj}$). Only if both tests were significant ($p < 0.05$), the dynamic cluster were included (Li and Curtis, 2023; Degutis et al., 2024; Spaak et al., 2017).

Bugs

For the first 11 participants, the number of images recorded in each run was set to 1448 instead of 1460, hence ending immediately after the last trial. Nineteen participants (pattern 1: 11, pattern 2: 8) had the same randomisation for the trial order due to a glitch in the code. The results did not change qualitatively after removing these participants from the analyses.

An earlier version of this manuscript included an analysis of serial order, where we reported a neural recency effect during the late delay period in sPCS, in both load conditions. This effect turned out to be due to a coding error and showed instead the decoding accuracy for the last two

scanner runs. The updated results of serial order can be found in Figure 2-2.

Results

Visual load selectively reduces mnemonic information in visual cortex

On trials with visual recall, participants performed better on trials where only the target item was an orientation and the other item was a pitch (visual Load 1, $precision = 0.079°$) compared to the visual Load 2 condition (visual Load 2, $precision = 0.070°, t_{(80)} = 2.98, p = 0.004$, Figure 1B and Figure 2-1A). To investigate this visual load effect on the distributed cortical representations, we decoded orientations continuously with a periodic support vector regression (pSVR Weber et al. (2024), see Methods and Figure 2A) from fMRI data. While all three regions of interest, the visual cortex (V1-V3), intraparietal sulcus (IPS) and precentral sulcus (sPCS), show information about orientations (Figure 2-1B) , the feature continuous accuracy (FCA) in each region changed with load and across time (Figure 2B).

The decoding accuracy in visual cortex was affected by visual load throughout the trial. Our results showed main effects of load ($F_{(1,80)} = 47.57, p < 0.0001$) and time ($F_{(1,80)} = 54.46, p < 0.0001$), as well as an interactions between load and time ($F_{(1,80)} = 14.16, p < 0.001$) on decoding accuracy. Early in the delay (7.2s-11.2s after first item onset)decoding accuracy decreased with increased visual working memory load ($t_{(80)} = -7.53, p < 0.0001$, Bonferroni corrected). In this early delay phase cortical representations can be assumed to be a mixture of perceptual and mnemonic representations due to the hemodynamic lag. However, the same pattern of results is also present late in the delay (12-16s after first item onset), when signals can be attributed only to working memory signals (12s-16s, see Rademaker et al. (2019); $t_{(80)} = -3.52, p = 0.002$, Bonferroni corrected). While in both conditions decoding accuracy dropped from early to late delay (Load 1: $t_{(80)} = 7.19, p < 0.0001$, Load 2: $t_{(80)} = 4.52, p < 0.0001$, Bonferroni corrected), it never dropped below chance (Figure 2B). On average, we found above chance decoding in both conditions in the early delay (Load 1: $t_{(80)} = 11.71, p < 0.0001$, Load 2: $t_{(80)} = 9.00, p < 0.0001$, uncorrected) and late delay (Load 1: $t_{(80)} = 7.50, p < 0.0001$, Load 2: $t_{(80)} = 5.61, p < 0.0001$, uncorrected).

Frontoparietal regions were not affected by load late in the delay. In IPS, our analysis revealed main effects of load ($F_{(1,80)} = 7.07, p = 0.009$) and time ($F_{(1,80)} = 7.81, p = 0.006$), as well as an interaction between load and time ($F_{(1,80)} = 5.39, p = 0.023$) on decoding accuracy. Here, decoding accuracy was reduced in visual Load 2 compared to Load 1 early, ($t_{(80)} = -3.50, p = 0.002$, Bonferroni corrected), but not late in the delay ($p = 1.0$, Bonferroni corrected). There was a significant difference in the change in decoding accuracy across time between load conditions. While

the decoding accuracy for representations in the visual Load 2 condition showed no difference between the early and late delay period in IPS ($p = 1$), the decoding accuracy for the single visual item dropped from early to late delay ($t_{(80)} = -3.29, p = 0.004$, Bonferroni corrected). There was above chance decoding in both conditions in the early delay (Load 1: $t_{(80)} = 7.03, p < 0.0001$, Load 2: $t_{(80)} = 4.29, p < 0.0001$, uncorrected) and late delay (Load 1: $t_{(80)} = 4.32, p < 0.0001$, Load 2: $t_{(80)} = 3.62, p = 0.0005$, uncorrected).

In sPCS, while there was above chance decoding in both delay periods and conditions, there was no significant difference in decoding accuracy between load conditions in either early (Above chance FCA in Load 1: $t_{(80)} = 2.94, p = 0.004$, Load 2: $t_{(80)} = 2.87, p = 0.005$, uncorrected; paired t-test $p > 0.8$, Bonferroni corrected) or late delay (Above chance FCA in Load 1: $t_{(80)} = 2.83, p = 0.006$, Load 2: $t_{(80)} = 2.39, p = 0.02$, uncorrected; paired t-test $p > 0.8$, Bonferroni corrected). There was no difference between early and late delay for either Load 1 (paired t-test $p > 0.9$) or Load 2 (paired t-test $p > 0.5$, Bonferroni corrected).

Decoding accuracy correlates with behavioural recall precision

Our results so far indicate that anterior as well as posterior regions store working memory representations. To quantify the contributions of the three regions to behavioural performance in each load condition, we correlated late delay decoding accuracy and behavioural precision across all participants. In V1-V3 ($r = 0.31, p = 0.005$) and sPCS ($r = 0.27, p = 0.014$) overall decoding accuracy correlated positively with behavioural precision, but not in IPS ($r = 0.22, p = 0.049$). Decodable information of orientations in visual cortex during the late delay correlated with behavioral performance in both visual load conditions ($r_{Load1} = 0.24, p = 0.03, r_{Load2} = 0.25, p = 0.02$). However, behavioural precision correlated significantly with decoding accuracy in IPS only in the Load 2 condition ($r = 0.28, p = 0.013$, Figure 2D), but not in the Load 1 condition ($r = 0.11, p = 0.34$). In sPCS, decoding accuracy correlated overall with behavioural precision, but not significantly for either Load 1 ($r = 0.12, p = 0.31$) or Load 2 ($r = 0.21, p = 0.06$). Further analysis comparing the correlations for each ROI showed that they are not significantly different from each other (all comparisons $p > 0.20$). A partial correlation revealed a unique contribution of decoding accuracy in visual cortex for behavioural precision in the visual Load 1 condition ($r = 0.25, p = 0.026$), but not with higher visual working memory load.

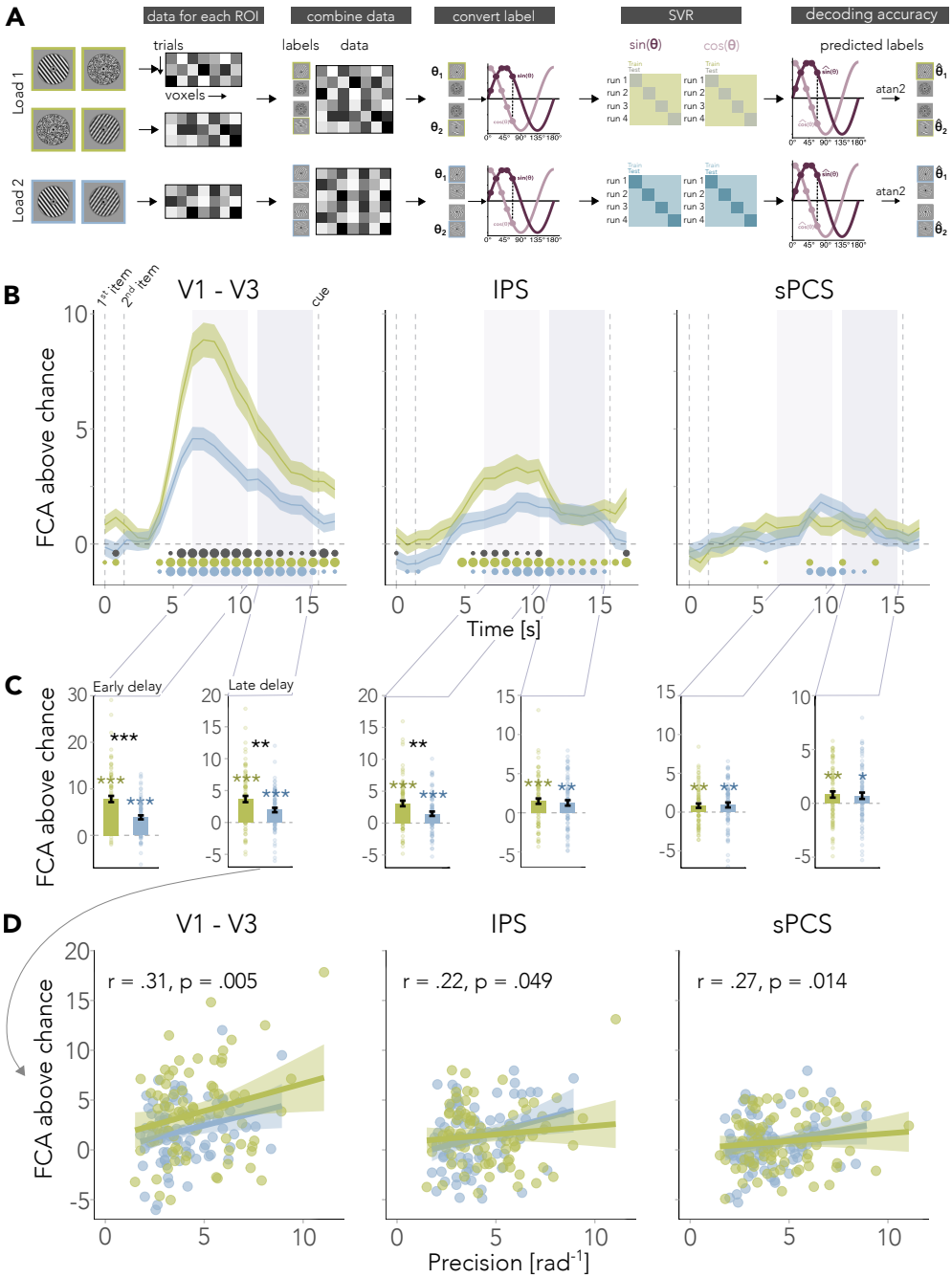

Figure 2: Decoding memorized orientations across cortical regions. **A** Analysis steps for each ROI. After selecting each trial for every condition, we combined trials and labels for both target and non-target orientations into one dataset. To change the circular orientations into linear labels, we converted the labels in degrees into sine and cosine labels. A support vector regression (SVR) was applied to predict the sine and cosine label separately(Weber et al., 2024). The difference between the orientation labels and predicted labels was converted into feature continuous accuracy (FCA). An FCA of 0% refers to chance level decoding of 45°. See Methods for details. **B** Time-course of item-specific decoding accuracy for each visual Load condition in all three ROIs. Early (7.2s-11.2s), where signals can be attributed to perceptual and mnemonic signals, and late delay (12s-16s), where signal can be attributed to working memory maintenance, after first item onset were chosen to avoid overlap. FCA above chance for the first and second item was averaged in each load condition. **C** Average difference between Load 1 and Load 2 in early and late delay. Asterisk above each bar indicate uncorrected above chance significance. **D** Correlations between late delay FCA and working memory recall precision. Correlation coefficient in figures refers to correlation across both conditions. Points in **C** and **D** represent single subjects. Dots (small, medium, large) at the bottom of **B** and asterisks in **C** indicate significance levels of $*p < .05$, $*p < .01$ or $***p < .001$. Shaded ribbons and error bars show SEM.

Simulations indicate different information content in visual versus anterior regions

Our results indicate that in visual cortex, but not in frontoparietal areas, decoding accuracy for orientations is reduced when multiple items are maintained in working memory. Brain-behaviour correlations suggest that visual cortex uniquely contributes to the storage of single visual items. This suggests distinct functional roles for these three cortical areas.

But is our pSVR analysis able to differentiate overlapping representations and quantify the strength of the underlying representations? We simulated multivariate patterns with our experimental parameters and compared a Load 1 condition to two variants of a Load 2 condition (see Methods and Figure 3A and B). First, we simulated multivariate patterns for a single orientation (Load 1) and two orientations by adding up the multivariate patterns for each orientation (Botvinick and Watanabe, 2007). In this scenario, we assume that in the Load 2 condition both items are maintained in the multivariate signal and thus a capacity of two (Load 2-Capacity 2). Secondly, we simulated a Load 2 condition where on each trial one of the two orientations was randomly selected to be maintained, thus simulating a capacity of one (Load 1-Capacity 1; see also Sutterer et al. (2019)). While we varied the signal strength overall, we kept the strength of concurrent items the same in all simulations.

Our results for the comparison between Load 1 and Load 2-Capacity 2, where the two patterns overlap, show that there is only a minor drop in FCA. This indicates that we can indeed decode information about orientations from overlapping patterns, if this drop is accounted for. On the other hand, FCA dropped substantially when we simulated a capacity of 1 (Load 2-Capacity 1, Figure 3C), indicating that a loss of information in the Load 2 condition can be identified with our methods.

How do these simulations compare to our empirical findings? We matched the simulated signal strength for each empirical Load 1 condition in each ROI and compared the ratio of FCA drop from Load 1 to Load 2 of our simulated results to our empirical results (Figure 3D and Methods). In the parietal and frontal cortex, our empirical results show high similarity to simulated results of a capacity of 2, where both items are concurrently maintained in working memory. This suggests that there is little cost to storing additional visual items in these regions. In visual cortex, empirical FCA dropped below the level expected when two orientations would be maintained (Load 2-capacity 2), but was higher than the FCA expected when only one of the items would be maintained (Load 2-Capacity 1), suggesting that more than one visual item can be maintained in V1-V3, but at a cost for the individual representations.

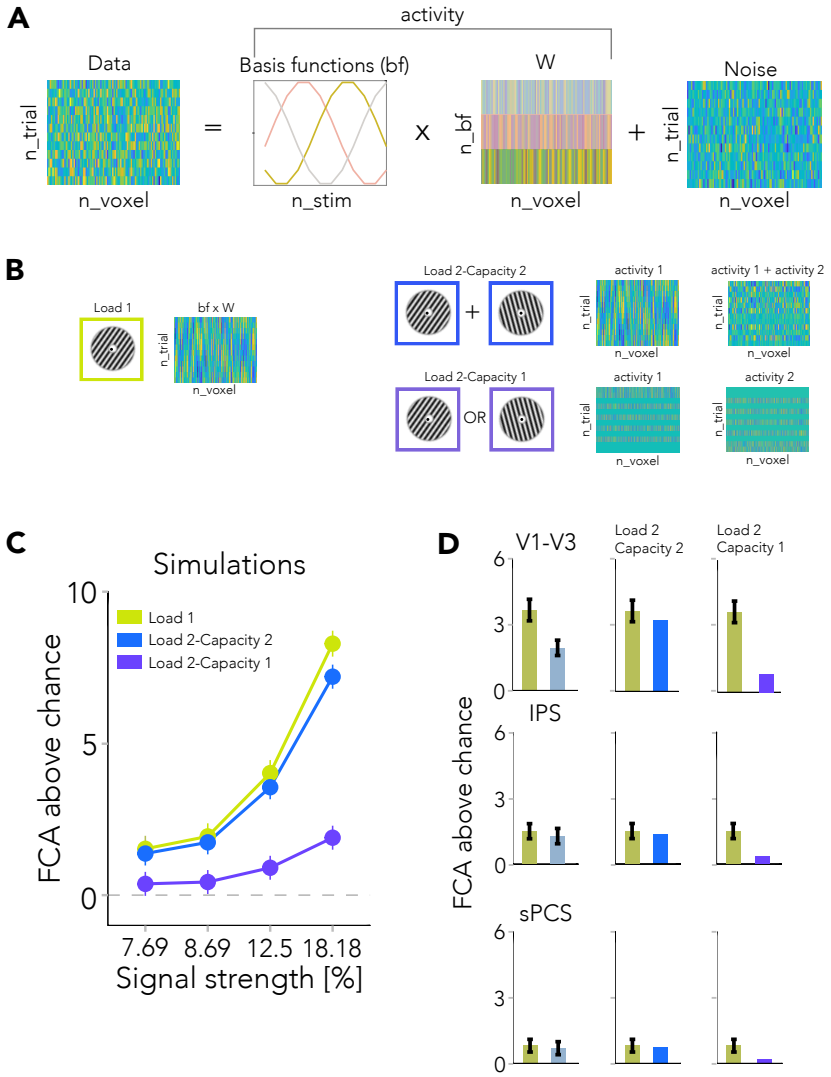

Figure 3: Simulated data show differences between capacity limits. **A** Schematic simulation pipeline. Simulated data for example trials, voxels and three basis functions. **B** Multivariate pattern for a single orientation. Addition of activity patterns for Load 2-Capacity 2 or random selection of a single pattern per trial for Load 2-Capacity 1. **C** FCA above chance for simulated load conditions across different signal strength levels. **D** Empirical FCA for Load 1 and 2 in late delay period (first column). Empirical Load 1 divided by ratios for simulated load conditions for each ROI. Errorbars show SEM.

Shared representations in visual cortex, distinct mnemonic code in sPCS

Considering that we observed changes in decoding accuracy across delay phases, we tested whether the neural code changes across time. First, we probed whether the multi-voxel pattern at one time-point generalizes to other time-points, within each load condition. Importantly, cross-decoding scales with the overall decoding accuracy, which limits the interpretability of these results.

When a single orientation (Load 1) is maintained in memory, the neural codes seemed to generalize between early and late delay time-points in all regions but sPCS(Figure 4A). In the Load 2 condition, temporal generalization is reduced, in accordance with the lower decoding accuracy

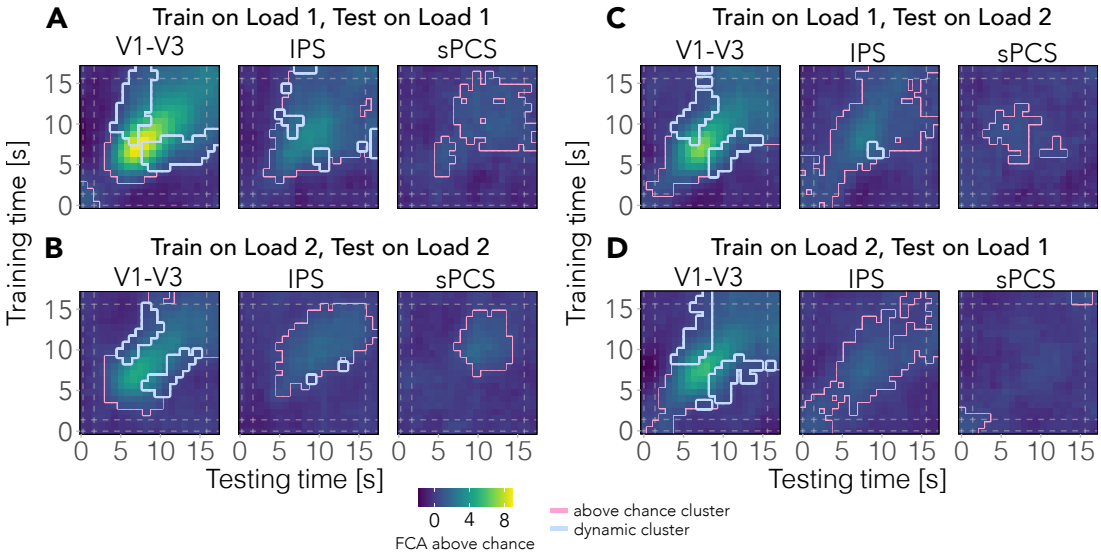

Figure 4: Mnemonic representations generalize between conditions in visual and parietal areas. Results for cross-condition temporal generalization, where we trained on each time-point in each load condition and tested on each time-point in the other load condition. Cross-temporal decoding for **A** Visual Load 1 and **B** Visual Load 2. Cross-temporal decoding when **C** training on TRs from Load 1 and testing on TRs from Load 2, and **D** training on TRs from Load 2 and testing on TRs from Load 1. White dotted lines indicate first item, second item and cue onset. Significant above chance clusters and dynamic clusters were tested for $p < 0.05$.

early in V1-V3 and IPS (Figure 4B). Temporal generalization in sPCS was limited to neighboring time-points later in the delay, potentially due to limitations in power.

In visual cortex, we find evidence for dynamic clusters, where off-diagonal accuracy is lower than both diagonal time-points, for both load conditions. The neural code in visual cortex seemed to be changing dynamically from perception to the maintenance period. The IPS showed fewer dynamic clusters, while no dynamic clusters were found in sPCS.

Next, we tested whether the neural code for orientations is shared between load conditions. We trained the pSVR on each time-point in one load condition and tested on each time-point in the other load condition. In visual and parietal cortex, we found significant cross-condition decoding (diagonal in Figure 4C and D), suggesting that these representations generalized well across conditions. In sPCS, cross-condition decoding appears to be lower than within-condition decoding.

Overall, these results suggest that cortical working memory representations generalize across time, but not without loss of representational precision. It is further possible that the low cross-condition decoding in sPCS indicates different neural codes used for mnemonic representations in the two load conditions in this regions.

Discussion

Visual working memory representations are distributed across the cortex (Fuster, 2006; Christophel et al., 2017). We investigated the effect of working memory load on these distributed representations by keeping the overall load constant at two items, but varying the sensory modality of each item. Our results suggest that the precision of visual working memory recall is limited by the resources available in visual cortex for the maintenance of multiple similar items. In contrast, increasing visual working memory load did not reduce item-specific information in IPS and sPCS during working memory maintenance. Item-specific decoding accuracy of this maintenance period predicted behavioural recall precision. Our cross-decoding and temporal generalization analyses hint at dynamic representational changes from perception to working memory in visual cortex and distinct mnemonic representations in frontal regions.

Previous studies showed that increasing visual working memory load reduces the ability to decode neural representations of remembered spatial locations and motion directions (Emrich et al., 2013; Sutterer et al., 2019). While these studies did not selectively investigate representations in visual cortex, the electrodes and voxels included in the respective analyses overlapped with occipital regions. When increasing visual working memory load for spatial locations, occipital and posterior parietal areas showed a decrease in strength of neural representations, which was also reflected in the decrease in behavioural performance (Sprague et al., 2014). These studies, as well as our task, encouraged the precise recall of low-level visual features and thus precise neural encoding in visual areas. However, the representations in visual cortex seem to be affected by interference between items, resulting in reduced decoding and thereby reduced behavioural precision. Simulations of multivariate pattern for one and two orientations (see also Botvinick and Watanabe (2007); Sutterer et al. (2019)), suggest that while both orientations (Load 2) are maintained in working memory signals in visual cortex, it comes with a loss of representational strength.

Frontoparietal memory representations were not disrupted by increased visual working memory load, consistent with prior studies showing distractor-resistant representations in these regions (Bettencourt and Xu, 2016; Lorenc et al., 2018; Rademaker et al., 2019; Hallenbeck et al., 2021). In parietal cortex, there was no difference in decoding accuracy between load conditions late in the delay. These representations might support working memory recall for low-level visual features at higher loads.

Our results show fewer dynamic clusters and lower cross-decoding between load conditions in these frontoparietal regions. Previous studies have shown suggested dynamic population coding in primate prefrontal areas could maintain stable working memory representations (Murray et al.,

2017; Spaak et al., 2017). In humans, visual areas appear to show stronger dynamic change in representations compared to frontoparietal areas when a single spatial location is maintained in working memory (Li and Curtis, 2023). However, the temporal generalization and cross-decoding results are confounded by the strength of decoding accuracy in each region. While decoding accuracy is not comparable across ROIs, as two-way decoding of working memory contents showed a lower base-rate in frontal areas compared to visual cortex (Bhandari et al., 2018), it is possible that decoders can pick up on the cortical retinotopy in visual cortex for orientations from multivoxel patterns (Sasaki et al., 2006; Freeman et al., 2011), but possibly not the abstract features stored by frontal neurons that are not retinotopically organized (Sreenivasan et al., 2014). If orientations are stored in a more abstract format in frontoparietal areas and even visual areas during the working memory delay (Chunharas et al., 2023; Yan et al., 2023; Kwak and Curtis, 2022; Duan and Curtis, 2024), our decoding method, which assumes a continuous feature space, would thus underestimate the amount of information decodable from the neural patterns. Further studies should seek to disentangle the effects of decoding information with different neural codes.

The mechanism for the drop in decoding accuracy in visual cortex from visual Load 1 to Load 2 needs to be considered separately from the absence thereof in frontoparietal regions. Our task required the maintenance of two items in each trial and frontoparietal regions have been implicated in maintaining modality independent representations (Spitzer and Blankenburg, 2012). Thus, another interpretation of our results could be that the resource is similarly distributed across the visual and auditory item in the visual Load 1 as for both visual items in the visual Load 2 condition (see Czoschke et al. (2021); Deutsch et al. (2023) for auditory decoding in these regions). Evidence from non-human primates shows a reduction in object information in these regions with increasing load (Buschman et al., 2011). Thus, future studies are required to indicate whether this drop and absence of a drop can be found when modulating only visual load in human fMRI work.

Our results suggest a division of labor, where visual cortices are important for the precise recall of individual low-level visual items and frontoparietal regions, which support the maintenance of multiple items in working memory. We demonstrate that visual working memory performance relies on the involvement of multiple cortical regions.

Author Contributions

VC and TC designed the study. VC collected the data. VC and TC performed data analysis. SW contributed software and materials. VC and TC wrote the manuscript.

Extended Data

Figures 1-1, 2-1 and 2-2

References

Ashburner, J., Barnes, G., Chen, C.-C., Daunizeau, J., Flandin, G., Friston, K., Kiebel, S., Kilner, J., Litvak, V., Moran, R. et al. (2014), 'Spm12 manual', *Wellcome Trust Centre for Neuroimaging, London, UK* **2464**(4).

Baddeley, A. (2003), 'Working memory: looking back and looking forward', *Nature reviews neuroscience* **4**(10), 829–839.

Bettencourt, K. C. and Xu, Y. (2016), 'Decoding the content of visual short-term memory under distraction in occipital and parietal areas', *Nature neuroscience* **19**(1), 150–157.

Bhandari, A., Gagne, C. and Badre, D. (2018), 'Just above chance: is it harder to decode information from prefrontal cortex hemodynamic activity patterns?', *Journal of cognitive neuroscience* **30**(10), 1473–1498.

Botvinick, M. and Watanabe, T. (2007), 'From numerosity to ordinal rank: A gain-field model of serial order representation in cortical working memory', *Journal of Neuroscience* **27**(32), 8636–8642.

Brainard, D. H. and Vision, S. (1997), 'The psychophysics toolbox', *Spatial vision* **10**(4), 433–436.

Buschman, T. J., Siegel, M., Roy, J. E. and Miller, E. K. (2011), 'Neural substrates of cognitive capacity limitations', *Proceedings of the National Academy of Sciences* **108**(27), 11252–11255.

Chang, C.-C. and Lin, C.-J. (2011), 'Libsvm: a library for support vector machines', *ACM transactions on intelligent systems and technology (TIST)* **2**(3), 1–27.

Christophel, T. B., Klink, P. C., Spitzer, B., Roelfsema, P. R. and Haynes, J.-D. (2017), 'The distributed nature of working memory', *Trends in cognitive sciences* **21**(2), 111–124.

Chunharas, C., Hettwer, M. D., Wolff, M. J. and Rademaker, R. L. (2023), 'A gradual transition from veridical to categorical representations along the visual hierarchy during working memory, but not perception.', *bioRxiv* pp. 2023–05.

Cohen, M. A., Konkle, T., Rhee, J. Y., Nakayama, K. and Alvarez, G. A. (2014), 'Processing multiple visual objects is limited by overlap in neural channels', *Proceedings of the National Academy of Sciences* **111**(24), 8955–8960.

Constantinidis, C., Franowicz, M. N. and Goldman-Rakic, P. S. (2001), 'The sensory nature of mnemonic representation in the primate prefrontal cortex', *Nature neuroscience* **4**(3), 311–316.

Czoschke, S., Fischer, C., Bahador, T., Bledowski, C. and Kaiser, J. (2021), 'Decoding concurrent representations of pitch and location in auditory working memory', *Journal of Neuroscience* **41**(21), 4658–4666.

Degutis, J. K., Weber, S., Soch, J. and Haynes, J.-D. (2024), 'Neural dynamics of visual working memory representation during sensory distraction', *bioRxiv* pp. 2024–04.

D'Esposito, M. (2007), 'From cognitive to neural models of working memory', *Philosophical Transactions of the Royal Society B: Biological Sciences* **362**(1481), 761–772.

Deutsch, P., Czoschke, S., Fischer, C., Kaiser, J. and Bledowski, C. (2023), 'Decoding of working memory contents in auditory cortex is not distractor-resistant', *Journal of Neuroscience* **43**(18), 3284–3293.

Diedenhofen, B. and Musch, J. (2015), 'cocor: A comprehensive solution for the statistical comparison of correlations', *PLoS ONE* **10**(4), e0121945.

Duan, Z. and Curtis, C. E. (2024), 'Visual working memories are abstractions of percepts', *Elife* **13**, RP94191.

Emrich, S. M., Riggall, A. C., LaRocque, J. J. and Postle, B. R. (2013), 'Distributed patterns of activity in sensory cortex reflect the precision of multiple items maintained in visual short-term memory', *Journal of Neuroscience* **33**(15), 6516–6523.

Ester, E. F., Anderson, D. E., Serences, J. T. and Awh, E. (2013), 'A neural measure of precision in visual working memory', *Journal of cognitive neuroscience* **25**(5), 754–761.

Ester, E. F., Sprague, T. C. and Serences, J. T. (2015), 'Parietal and frontal cortex encode stimulus-specific mnemonic representations during visual working memory', *Neuron* **87**(4), 893–905.

Franconeri, S. L., Alvarez, G. A. and Cavanagh, P. (2013), 'Flexible cognitive resources: competitive content maps for attention and memory', *Trends in cognitive sciences* **17**(3), 134–141.

Freeman, J., Brouwer, G. J., Heeger, D. J. and Merriam, E. P. (2011), 'Orientation decoding depends on maps, not columns', *Journal of Neuroscience* **31**(13), 4792–4804.

Funahashi, S., Bruce, C. J. and Goldman-Rakic, P. S. (1989), 'Mnemonic coding of visual space in the monkey's dorsolateral prefrontal cortex', *Journal of neurophysiology* **61**(2), 331–349.

Fuster, J. M. (1998), 'Distributed memory for both short and long term', *Neurobiology of learning and memory* **70**(1-2), 268–274.

Fuster, J. M. (2006), 'The cognit: a network model of cortical representation', *International Journal of Psychophysiology* **60**(2), 125–132.

Fuster, J. M. and Jervey, J. P. (1981), 'Inferotemporal neurons distinguish and retain behaviorally relevant features of visual stimuli', *Science* **212**(4497), 952–955.

Goldman-Rakic, P. S. (1995), 'Cellular basis of working memory', *Neuron* **14**(3), 477–485.

Gorgoraptis, N., Catalao, R. F., Bays, P. M. and Husain, M. (2011), 'Dynamic updating of working memory resources for visual objects', *Journal of Neuroscience* **31**(23), 8502–8511.

Hallenbeck, G. E., Sprague, T. C., Rahmati, M., Sreenivasan, K. K. and Curtis, C. E. (2021), 'Working memory representations in visual cortex mediate distraction effects', *Nature Communications* **12**(1), 4714.

Harrison, S. A. and Tong, F. (2009), 'Decoding reveals the contents of visual working memory in early visual areas', *Nature* **458**(7238), 632–635.

Hebart, M. N., Görgen, K. and Haynes, J.-D. (2015), 'The decoding toolbox (tdt): a versatile software package for multivariate analyses of functional imaging data', *Frontiers in neuroinformatics* **8**, 88.

Kiyonaga, A. and D'Esposito, M. (2020), *Competition and Control during Working Memory*, Cambridge University Press.

Kwak, Y. and Curtis, C. E. (2022), 'Unveiling the abstract format of mnemonic representations', *Neuron* **110**(11), 1822–1828.

Leavitt, M. L., Pieper, F., Sachs, A. J. and Martinez-Trujillo, J. C. (2018), 'A quadrantic bias in prefrontal representation of visual-mnemonic space', *Cerebral Cortex* **28**(7), 2405–2421.

Li, H.-H. and Curtis, C. E. (2023), 'Neural population dynamics of human working memory', *Current Biology* **33**(17), 3775–3784.

Lorenc, E. S., Sreenivasan, K. K., Nee, D. E., Vandenbroucke, A. R. and D'Esposito, M. (2018), 'Flexible coding of visual working memory representations during distraction', *Journal of Neuroscience* **38**(23), 5267–5276.

Luck, S. J. and Vogel, E. K. (1997), 'The capacity of visual working memory for features and conjunctions', *Nature* **390**(6657), 279–281.

Ma, W. J., Husain, M. and Bays, P. M. (2014), 'Changing concepts of working memory', *Nature neuroscience* **17**(3), 347–356.

Maris, E. and Oostenveld, R. (2007), 'Nonparametric statistical testing of eeg-and meg-data', *Journal of neuroscience methods* **164**(1), 177–190.

Murray, J. D., Bernacchia, A., Roy, N. A., Constantinidis, C., Romo, R. and Wang, X.-J. (2017), 'Stable population coding for working memory coexists with heterogeneous neural dynamics in prefrontal cortex', *Proceedings of the National Academy of Sciences* **114**(2), 394–399.

Overkott, C. and Souza, A. S. (2022), 'Verbal descriptions improve visual working memory but have limited impact on visual long-term memory.', *Journal of Experimental Psychology: General* **151**(2), 321.

Pilly, P. K. and Seitz, A. R. (2009), 'What a difference a parameter makes: A psychophysical comparison of random dot motion algorithms', *Vision research* **49**(13), 1599–1612.

Rademaker, R. L., Chunharas, C. and Serences, J. T. (2019), 'Coexisting representations of sensory and mnemonic information in human visual cortex', *Nature neuroscience* **22**(8), 1336–1344.

Sasaki, Y., Rajimehr, R., Kim, B. W., Ekstrom, L. B., Vanduffel, W. and Tootell, R. B. (2006), 'The radial bias: a different slant on visual orientation sensitivity in human and nonhuman primates', *Neuron* **51**(5), 661–670.

Serences, J. T., Ester, E. F., Vogel, E. K. and Awh, E. (2009), 'Stimulus-specific delay activity in human primary visual cortex', *Psychological science* **20**(2), 207–214.

Spaak, E., Watanabe, K., Funahashi, S. and Stokes, M. G. (2017), 'Stable and dynamic coding for working memory in primate prefrontal cortex', *Journal of neuroscience* **37**(27), 6503–6516.

Spitzer, B. and Blankenburg, F. (2012), 'Supramodal parametric working memory processing in humans', *Journal of Neuroscience* **32**(10), 3287–3295.

Sprague, T. C., Boynton, G. M. and Serences, J. T. (2019), 'The importance of considering model choices when interpreting results in computational neuroimaging', *ENeuro* **6**(6).

Sprague, T. C., Ester, E. F. and Serences, J. T. (2014), 'Reconstructions of information in visual spatial working memory degrade with memory load', *Current Biology* **24**(18), 2174–2180.

Sreenivasan, K. K., Curtis, C. E. and D'Esposito, M. (2014), 'Revisiting the role of persistent neural activity during working memory', *Trends in cognitive sciences* **18**(2), 82–89.

Sutterer, D. W., Foster, J. J., Adam, K. C., Vogel, E. K. and Awh, E. (2019), 'Item-specific delay activity demonstrates concurrent storage of multiple active neural representations in working memory', *PLoS biology* **17**(4), e3000239.

Wang, L., Mruczek, R. E., Arcaro, M. J. and Kastner, S. (2015), 'Probabilistic maps of visual topography in human cortex', *Cerebral cortex* **25**(10), 3911–3931.

Weber, S., Christophel, T., Görgen, K., Soch, J. and Haynes, J.-D. (2024), 'Working memory signals in early visual cortex are present in weak and strong imagers', *Human brain mapping* **45**(4), e26590.

Welvaert, M. and Rosseel, Y. (2014), 'A review of fmri simulation studies', *PloS one* **9**(7), e101953.

Wimmer, K., Nykamp, D. Q., Constantinidis, C. and Compte, A. (2014), 'Bump attractor dynamics in prefrontal cortex explains behavioral precision in spatial working memory', *Nature neuroscience* **17**(3), 431–439.

Wing, E. A., Burles, F., Ryan, J. D. and Gilboa, A. (2022), 'The structure of prior knowledge enhances memory in experts by reducing interference', *Proceedings of the National Academy of Sciences* **119**(26), e2204172119.

World Medical Association (2013), 'World medical association declaration of helsinki: ethical principles for medical research involving human subjects', *Jama* **310**(20), 2191–2194.

Xu, Y. (2023), 'Parietal-driven visual working memory representation in occipito-temporal cortex', *Current biology* **33**(20), 4516–4523.

Yan, C., Christophel, T. B., Allefeld, C. and Haynes, J.-D. (2023), 'Categorical working memory codes in human visual cortex', *NeuroImage* **274**, 120149.

Extended Data

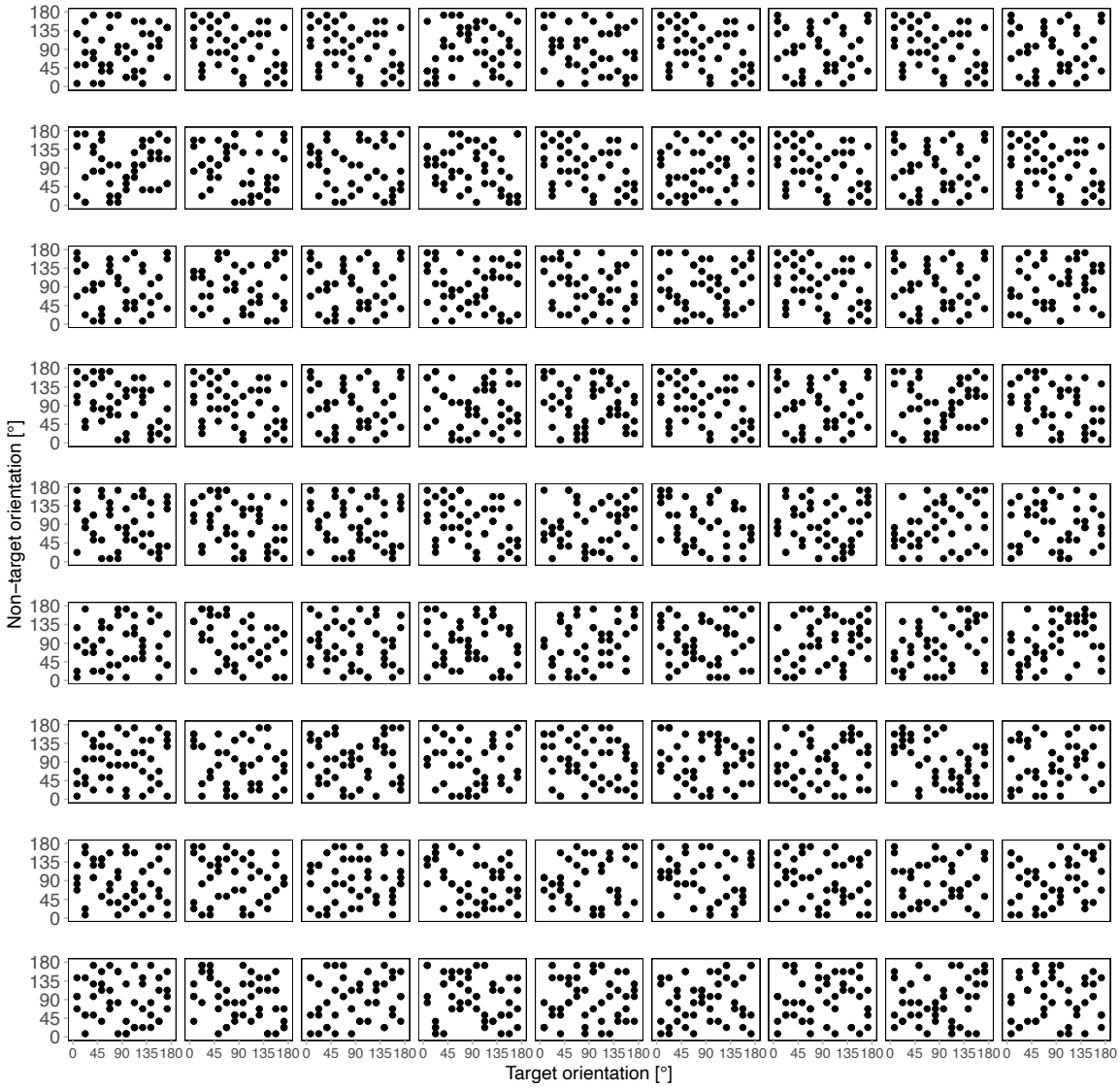

Figure 1 - 1: Scatterplots for each participant showing target and non-target orientations in Load 2 condition.

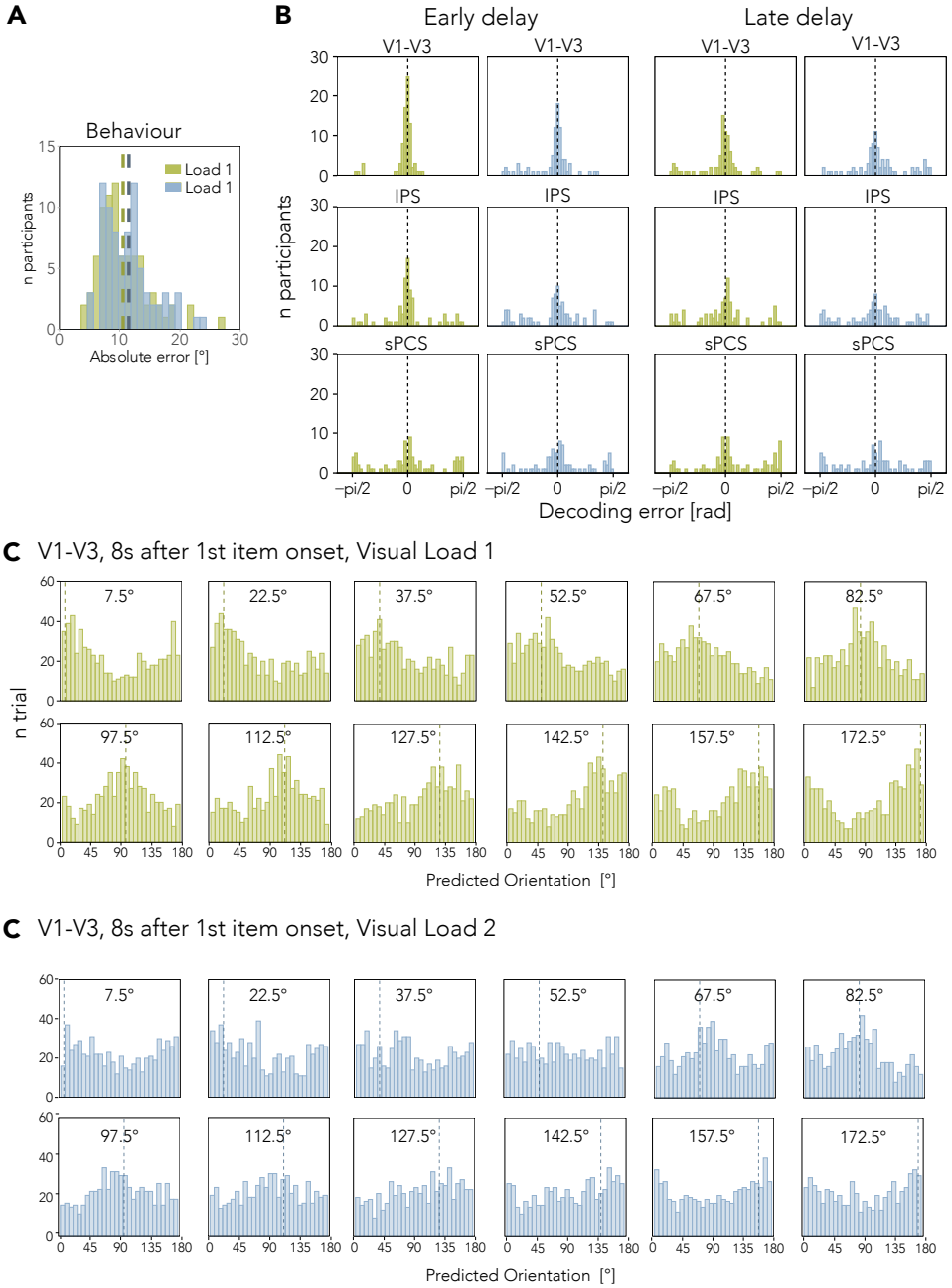

Figure 2 - 1: Histograms across participants and trials. **A** Absolute recall error. Recall performance dropped 10%, from 10.57° (SEM = 0.46°) in Load 1 to 11.54° (SEM = 0.45°) in Load 2. Dotted lines show these means for each condition. **B** Decoding error in radians for each ROI, delay period (early delay: 7.2s-11.2s; late delay: 12s-16s) and condition.Example for trial-wise decoding for each orientation in Visual Cortex at the perceptual peak (8s after first item onset) for **C** Visual Load 1 and **D** Visual Load 2. Dotted line and degrees inside the boxes show the presented orientation, bars refer to trial count across participants

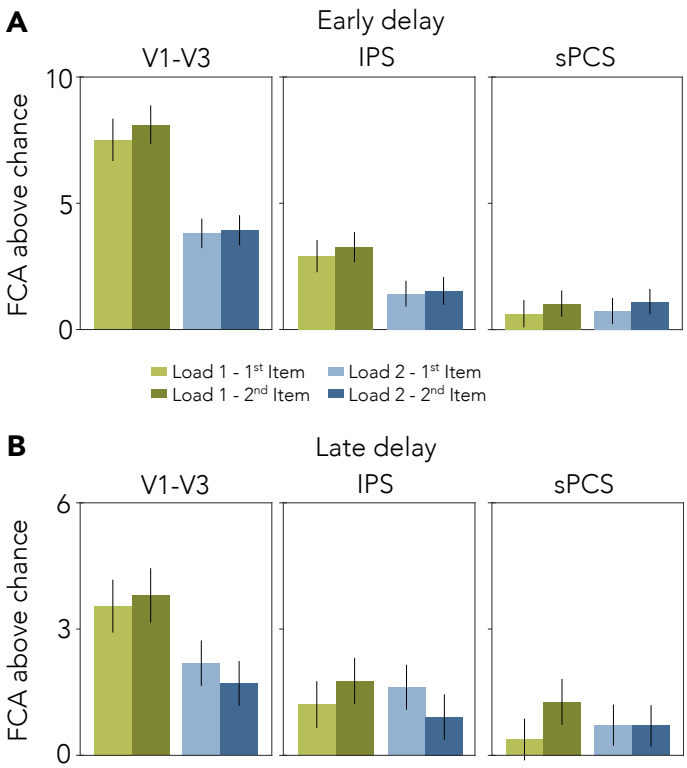

Figure 2 - 2: Serial order analysis. **A** FCA above chance for the early delay (7.2s-11.2s after first item onset) for each item and load condition. In V1-V3, accuracy was above chance for each item position in each load condition (Load 1, 1st item: $t_{(80)} = 10.09, p < 0.001$, Load 1, 2nd item: $t_{(80)} = 11.96, p < 0.001$, Load 2, 1st item: $t_{(80)} = 7.83, p < 0.001$, Load 2, 2nd item: $t_{(80)} = 7.75, p < 0.001$). There was no difference between item positions (all $p > 0.54$). Similarly, in IPS there was no difference between item positions (all $p > 0.6$ but significant decoding above chance (Load 1, 1st item: $t_{(80)} = 5.52, p < 0.001$, Load 1, 2nd item: $t_{(80)} = 6.95, p < 0.001$, Load 2, 1st item: $t_{(80)} = 3.55, p < 0.001$, Load 2, 2nd item: $t_{(80)} = 3.36, p = 0.001$). In sPCS, there was significant decoding for the 2nd items (Load 1, 1st item: $t_{(80)} = 1.79, p = 0.077$, Load 1, 2nd item: $t_{(80)} = 2.85, p = 0.006$, Load 2, 1st item: $t_{(80)} = 1.86, p = 0.067$, Load 2, 2nd item: $t_{(80)} = 2.89, p = 0.005$), but no significant difference between first and second item (all $p > 0.4$).
B Reconstruction accuracy for the late delay (12s-16s after first item onset). There was no significant difference in FCA for each item. In V1-V3, there was significant above chance decoding for both items in both load conditions (Load 1, 1st item: $t_{(80)} = 6.60, p < 0.001$, Load 1, 2nd item: $t_{(80)} = 7.24, p < 0.001$, Load 2, 1st item: $t_{(80)} = 4.88, p < 0.001$, Load 2, 2nd item: $t_{(80)} = 3.91, p < 0.001$), and no difference between the first and second item (all $p > 0.4$). In IPS, there was significant decoding for the first and second item in both load conditions (Load 1, 1st item: $t_{(80)} = 2.70, p = 0.008$, Load 1, 2nd item: $t_{(80)} = 4.14, p < 0.001$, Load 2, 1st item: $t_{(80)} = 3.78, p < 0.001$, Load 2, 2nd item: $t_{(80)} = 2.05, p = 0.04$), and no difference between item positions (all $p > 0.25$). In sPCS, there was some significant above chance decoding (Load 1, 1st item: $t_{(80)} = 1.06, p = 0.29$, Load 1, 2nd item: $t_{(80)} = 3.15, p = 0.002$, Load 2, 1st item: $t_{(80)} = 1.94, p = 0.06$, Load 2, 2nd item: $t_{(80)} = 1.83, p = 0.07$) and no difference between the first and second item in either load condition (all $p > 0.09$).
Error bars show the SEM. P-values are uncorrected for multiple comparisons. Asterisks indicate significance levels of $*p < .05$, $*p < .01$ or $***p < .001$.